Ocean Engineering 75 (2014) 1–14

Contents lists available at ScienceDirect

Ocean Engineering

journal homepage: www.elsevier.com/locate/oceaneng

Nonlinear hull girder loads of a RoPax ship

Timo Kukkanen [a,*], Jerzy Matusiak [b]

[a] VTT Technical Research Centre of Finland, Tietotie 1 A, Espoo, PO Box 1000, FI-02044 VTT, Finland
[b] Aalto University, School of Engineering, Department of Applied Mechanics, Tietotie 1 A, Espoo, PO Box 15300, FI-00076 Aalto, Finland

ARTICLE INFO

Article history:
Received 5 March 2013
Accepted 18 October 2013
Available online 19 November 2013

Keywords:
Seakeeping
Nonlinear panel method
Hull girder loads
Model tests

ABSTRACT

Numerical and experimental studies of nonlinear wave loads are presented. A nonlinear time domain method has been developed and the theoretical background of the method are provided. The method is based on the source formulation expressed by means of the transient three-dimensional Green function. The time derivative of the velocity potential in Bernoulli's equation is solved with a similar source formulation to that of the perturbation velocity potential. The Wigley hull form is used to validate the calculation method in regular head waves. Model tests of a roll-on roll-off passenger ship with a flat bottom stern have been carried out. Model test results of ship motions, vertical shear forces and bending moments in regular and irregular head waves and calm water are given. The nonlinearities in ship motions and hull girder loads are investigated using the calculation method and the model test results. The nonlinearities in the hull girder loads have been found to be significant and the calculation method can predict the nonlinear loads for the model test ship.

1. Introduction

In the structural analyses of ships, an accurate prediction of extreme wave loads is important in the ultimate strength assessment of the hull girder. Direct calculations of wave loads in structural analyses of ships are generally based on linear theories expressed in the frequency domain. In the linear methods, the ship motions and wave amplitudes are assumed to be small, and the body and free surface boundary conditions can be linearised. In high waves, the linearity assumption of wave loads with respect to wave height is not usually valid. In the structural design of ships, it is common practice to express the extreme design wave loads by means of the sagging and hogging bending moments and shear forces. For ships in heavy seas, the sagging loads are greater than the hogging loads.

Recently, several different approaches have been developed to take nonlinearities in wave load predictions into account. A summary of different methods in seakeeping computations is given by Beck and Reed (2000). A two-dimensional method for large-amplitude ship motions and wave loads was presented by Fonesca and Guedes Soares (1998). The method was based on a strip-theory approach, and the radiation and diffraction forces and moments were linear. Nonlinear effects were included in hydrostatic restoring and Froude–Krylov forces and moments. A quadratic strip theory was applied by Jensen et al. (2008) to determine extreme hull girder loads on container ships. A nonlinear hydroelastic method based on a two-dimensional strip theory was presented by Wu and Moan (1996, 2005). Model test results for a container ship in regular and irregular oblique waves and calculated results were presented by Drummen et al. (2009) and Zhu et al. (2011). Time domain three-dimensional linear and nonlinear methods based on a transient Green function were presented by Ferrant (1991), Lin and Yue (1991), Kataoka et al. (2002) and Sen (2002). The time domain representation of the Green function allows the exact body boundary condition to be applied. This means that pressures can be solved in the actual floating position of the body and not only on the mean wetted surface. For example, the exact body boundary condition is satisfied in the seakeeping program LAMP (Lin and Yue, 1991). A nonlinear Rankine source method applying a weak-scatterer hypothesis (Pawlowski, 1992) was presented by Huang and Sclavounos (1998). In the weak-scatterer hypothesis, the disturbance due to the ship's motions in the wave flow is assumed to be small compared to the wave flow due to the incoming wave. Model tests and computations by the Rankine source method for the motions and loads of the container ship were given by Song et al. (2011). Koo and Kim (2004) presented a two-dimensional nonlinear method in which the fluid flow was solved with two-dimensional Rankine sources. The boundary condition at the free surface was nonlinear and the exact body boundary condition was satisfied on the body surface. They applied an acceleration-potential formulation to solve the time derivative of the velocity potential in Bernoulli's equation (Tanizawa, 1995). Two- and three-dimensional methods based on the Rankine sources

* Corresponding author. Tel.: +358 20 722 6237.
E-mail addresses: timo.kukkanen@vtt.fi (T. Kukkanen), jerzy.matusiak@aalto.fi (J. Matusiak).

0029-8018/$ - see front matter © 2013 Elsevier Ltd. All rights reserved.
http://dx.doi.org/10.1016/j.oceaneng.2013.10.008

were presented by Zhang et al. (2010). The exact body boundary condition was used and the free surface boundary condition was linear. A hybrid formulation was presented by Dai and Wu (2008) and Weems et al. (2000). They used the transient Green function on the outer domain and Rankine sources in the inner domain to solve the velocity potential. Close to the free surface, the transient Green function is a strongly oscillating function. The oscillation can induce instabilities in the solution; especially if the body has horizontal body shapes or the inclination angle of the body shapes are small at the free surface. The instability in the transient Green function solution was studied by, for example, Duan and Dai (1999), and Datta et al. (2011). Applying the hybrid formulation, the possible instabilities in the transient Green function solution can be avoided. Kataoka and Iwashita (2004) presented a hybrid method in which the artificial boundary between the outer and inner domain was expressed in the space-fixed coordinate system.

A nonlinear time domain calculation method is presented in this paper. A method to solve the time derivative of the velocity potential, i.e. the acceleration potential, in Bernoulli's equation is presented. The solution is based on the same source formulation and transient Green function as the boundary value problem for the perturbation velocity potential but with a different body boundary condition. The boundary and initial value problems for the perturbation velocity potential are similar to those given by Ferrant (1991), Lin and Yue (1991) and Sen (2002). The solution of the boundary value problem is based on source distributions on the body surface. The source distributions are represented with a transient three-dimensional Green function. The solution of the boundary value problem is expressed in the space-fixed coordinate system. The time domain computer program includes the solutions of the exact and linear body boundary conditions. The free surface boundary condition is linear. In the nonlinear calculation, the instantaneous position of the ship with respect to the mean water level is updated at every time step. Details of the calculation method are presented by Kukkanen (2012). The experimental results of the Wigley hull form are used to validate the calculation method in regular waves. Model tests of a roll-on roll-off passenger (RoPax) ship are presented. The ship model has a flat bottom stern at the waterline (counter stern). Model test results of ship motions and vertical shear forces and bending moments in regular and irregular head waves are given. Model test results in calm water at different forward speeds are also presented for sinkage of the ship and for steady vertical shear forces and bending moments.

2. Methods

2.1. Boundary value problem

Two coordinate systems are used: a space-fixed coordinate system $Oxyz$ and a body-fixed coordinate system $Ox_0y_0z_0$. The coordinate systems are shown in Fig. 1. The space-fixed coordinate system is the inertial reference frame. The origin of the space-fixed coordinate system is at the calm water plane with the z-axis pointing vertically upwards. The forward speed of the body is U_0. The forward speed is defined as the speed of the centre of gravity of the body and the body moving at speed U_0 parallel to the direction of the x-axis if the other motions in the y- and z-directions are zero. The longitudinal coordinate x_0 of the body-fixed coordinate system is pointing to the bow of the body and the z_0-axis is pointing vertically upwards. The origin of the body-fixed coordinate system is at the centre of gravity of the body. The incoming waves are travelling with angle χ with respect to the x-axis and the heading angle of $\chi=180$ degrees corresponds to head sea. The six degrees of freedom body motions are surge (η_1), sway (η_2), heave (η_3), roll (η_4), pitch (η_5) and yaw (η_6), defined with respect to the space-fixed coordinate system. The translational motions surge, sway and heave define the position of the centre of gravity of the body in the space-fixed coordinate system. The surge velocity $\dot{\eta}_1$ includes the forward speed U_0. Normal vectors are defined as positive, pointing out of the fluid. The boundary value problem is expressed in the space-fixed coordinate system.

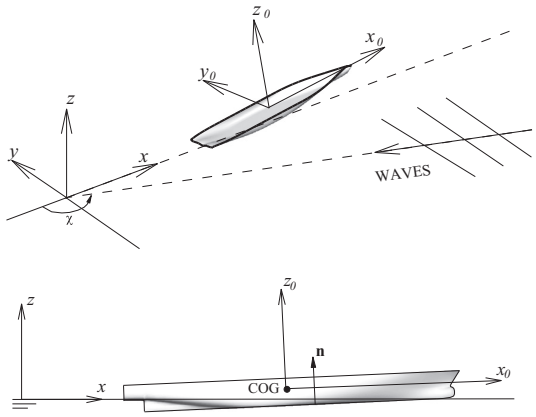

Fig. 1. Coordinate systems used in the time domain method.

It is assumed that the fluid is inviscid and the fluid density ρ is constant. Hence, for the irrotational flow, the fluid velocity is given by the velocity potential Φ. The velocity potential is expressed as a decomposition of the perturbation and incoming wave velocity potentials

$$\Phi = \phi + \phi_I, \tag{1}$$

where the perturbation velocity potential is ϕ and the velocity potential of the incoming wave is ϕ_I. The velocity potential ϕ has to satisfy Laplace's equation

$$\nabla^2\phi = 0, \tag{2}$$

everywhere in the fluid. On the free surface S_F ($z=0$), the linear free surface boundary condition is given by

$$\frac{\partial^2\phi}{\partial t^2} + g\frac{\partial\phi}{\partial z} = 0, \quad \text{on} \quad S_F. \tag{3}$$

The boundary condition on the body surface S_B is given as follows:

$$\frac{\partial\phi}{\partial n} = \mathbf{U}\cdot\mathbf{n} - \frac{\partial\phi_I}{\partial n}, \quad \text{on} \quad S_B, \tag{4}$$

where $\mathbf{n}$ is the unit normal to the body pointing out of the fluid and $\mathbf{U}$ is the velocity of the point on the body surface. The boundary condition on the sea bottom is given by the condition

$$\frac{\partial\phi}{\partial n} = 0, \quad z\to-\infty. \tag{5}$$

hence, an infinite water depth is assumed. The radiation condition takes into account the fact that the body-generated waves are progressing outwards and vanish at infinity

$$\frac{\partial\phi}{\partial n}\to 0, \quad r\to\infty, \tag{6}$$

where $r=\sqrt{x^2+y^2}$. In addition to the boundary conditions, the boundary value problem has to satisfy the following initial conditions:

$$\phi=0 \quad \text{and} \quad \frac{\partial\phi}{\partial t}=0 \quad \text{at} \quad t=0, \tag{7}$$

i.e. the fluid flow is not disturbed by the body at $t=0$.

The velocity potential of the incoming wave satisfies Laplace's equation, the linear boundary condition at the free surface and the bottom boundary condition. The velocity potential of the deep water linear wave can be given in the following form:

$$\phi_I=Re\left\{i\frac{ga}{\omega}e^{-i(kx\ \cos\ \chi+ky\ \sin\ \chi)}e^{kz}e^{i\omega t}\right\} \tag{8}$$

where a is the wave amplitude, ω is the wave frequency, and k is the wave number.

In the body nonlinear solution, the exact body boundary condition is used and the perturbation potential is solved at the actual floating position of the body. The body boundary condition is applied to the instantaneous wetted surface $S_B(t)$ on $z<0$. In the body boundary condition (4), the instantaneous normal component of the velocity of the point on the body surface is given by

$$\mathbf{U}\cdot\mathbf{n}=(\mathbf{u}+\boldsymbol{\omega}\times\mathbf{r})\cdot\mathbf{n} \tag{9}$$

where the position vector $\mathbf{r}$ of the point on the body surface and the translational and rotational velocities $\mathbf{u}$ and $\boldsymbol{\omega}$, respectively, are given in the body-fixed coordinate system. Hence, the normal vector $\mathbf{n}$ is also expressed in the body-fixed coordinate system. Thus, all the vector operations are performed in the same coordinate system.

2.2. Boundary condition of the acceleration potential

The boundary value problem for the velocity potential given in the previous section does not give a direct solution for the acceleration potential, i.e. the time derivative of the velocity potential $\phi_t=\partial\phi/\partial t$ in Bernoulli's equation. In the time domain methods, the acceleration potential is often solved using numerical methods such as a backward difference method (see for example Lin and Yue, 1991; Sen, 2002). The solution of the time derivative of the velocity potential can also be determined by solving a boundary value problem defined for the acceleration potential. Different methods have been developed to solve ϕ_t and the differences in the methods depend on the applied boundary conditions and the solution methods, such as Rankine source methods, that have been used. A review and comparison of different acceleration-potential methods applied to the fluid and body interaction problems were given by Bandyk and Beck (2011). One method is to solve $\phi_t=+\mathrm{U}\cdot\nabla\phi$, i.e. solving the substantial derivative of ϕ instead of solving ϕ_t directly. Vinje and Brevig (1981) applied this method to calculate motions of two-dimensional bodies, and Kang and Gong (1990) provided a solution for three-dimensional free surface problems. Greco (2001) applied a similar approach, studying a two-dimensional green water loading. Tanizawa (1995) developed a solution for the acceleration potential starting from the fluid acceleration. Wu (1998) derived a boundary condition for the acceleration potential, using the body boundary condition of the velocity potential as a starting point. A similar boundary condition for the acceleration potential was presented by Bandyk and Beck (2011). They also showed calculation results for two-dimensional bodies for which the velocity and acceleration potentials were solved using Rankine sources.

In this paper, a boundary condition for the acceleration potential is derived that can be used in the time domain method in the body nonlinear and linear solutions. The same approach was applied by Kang and Gong (1990) to represent the problem by the substantial derivative of ϕ instead of solving ϕ_t directly. However, the present boundary condition also includes terms due to the incident wave potential ϕ_t. The terms describing the body motions are the same as those presented by Wu (1998) and Kang and Gong (1990).

The boundary condition for the acceleration potential is derived from the body boundary condition (4). Taking the absolute time derivative in the inertial reference frame from both sides of the body boundary condition for the velocity potential ϕ, it follows that

$$\frac{d}{dt}\left(\frac{\partial\phi}{\partial n}\right)=\frac{d}{dt}[(\mathbf{U}-\nabla\phi_I)\cdot\mathbf{n}]\text{ on }\quad S_B. \tag{10}$$

The left-hand side of the above equation can be written as

$$\frac{d}{dt}\left(\frac{\partial\phi}{\partial n}\right)=\frac{d}{dt}(\mathbf{n}\cdot\nabla\phi)\mathbf{n}\cdot\frac{d}{dt}(\nabla\phi)+\frac{d\mathbf{n}}{dt}\cdot\nabla\phi \tag{11}$$

The time derivative of the normal vector is $dn/dt=\boldsymbol{\omega}\times\mathbf{n}$. For the fluid term, the time derivative is evaluated following the fluid on the fixed point on the body surface. Hence, the time derivative is given by the substantial derivative and Eq. (11) can be written as follows:

$$\frac{d}{dt}\left(\frac{\partial\phi}{\partial n}\right)=\mathbf{n}\cdot\left[\frac{\partial\nabla\phi}{\partial t}+(\mathbf{U}\cdot\nabla)\cdot\nabla\phi\right]+(\boldsymbol{\omega}\times\mathbf{n})\cdot\nabla\phi \tag{12}$$

The term $(\mathbf{U}\times\nabla)\times\nabla\phi$, where $\mathbf{U}=\mathbf{u}+\boldsymbol{\omega}\times\mathbf{r}$, can be further simplified using a vector identity (Milne-Thomson, 1968, p. 46, 2–34 III) and taking into account the fact that the flow is irrotational. The following result is obtained:

$$(\mathbf{U}\cdot\nabla)\nabla\phi=\nabla(\mathbf{U}\cdot\nabla\phi)-2\nabla\phi\times\boldsymbol{\omega}+(\nabla\phi\times\boldsymbol{\omega}). \tag{13}$$

Substituting this back into Eq. (12) gives

$$\begin{aligned}\frac{d}{dt}\left(\frac{\partial\phi}{\partial n}\right)&=\mathbf{n}\cdot\left[\frac{\partial\nabla\phi}{\partial t}+\nabla(\mathbf{U}\cdot\nabla\phi)+\boldsymbol{\omega}\times\nabla\phi\right]+(\boldsymbol{\omega}\times\mathbf{n})\cdot\nabla\phi\\&=\mathbf{n}\cdot\nabla\left(\frac{\partial\phi}{\partial t}+\mathbf{U}\cdot\nabla\phi\right)=\frac{\partial}{\partial n}\left(\frac{d\phi}{dt}\right).\end{aligned} \tag{14}$$

Furthermore, defining a potential function φ as follows:

$$\varphi=\frac{\partial\phi}{\partial t}+\mathbf{U}\cdot\nabla\phi=\frac{d\phi}{dt}, \tag{15}$$

then Eq. (14) can also be given as follows:

$$\frac{d}{dt}\left(\frac{\partial\phi}{\partial n}\right)=\frac{\partial\varphi}{\partial n} \tag{16}$$

hence, the left-hand side of Eq. (10) is the normal derivative of the potential function φ. The right-hand side of Eq. (10) is

$$\frac{d}{dt}[(\mathbf{U}-\nabla\phi_I)\cdot\mathbf{n}]=\frac{d}{dt}(\mathbf{U}\cdot\mathbf{n})-\frac{d}{dt}(\nabla\phi_I\cdot\mathbf{n}) \tag{17}$$

The velocity of the point on the body surface in the normal direction can be written as follows:

$$\begin{aligned}\frac{d}{dt}(\mathbf{U}\cdot\mathbf{n})&=\frac{d}{dt}[(\mathbf{u}+\boldsymbol{\omega}\times\mathbf{r})\cdot\mathbf{n}]\\&=(\dot{\mathbf{u}}+\dot{\boldsymbol{\omega}}\times\mathbf{r})\cdot\mathbf{n}-(\boldsymbol{\omega}\times\mathbf{u})\cdot\mathbf{n}\end{aligned} \tag{18}$$

where the translational acceleration vector of the centre of gravity of the body is $\dot{\mathbf{u}}$ and the angular acceleration vector of the body is $\dot{\boldsymbol{\omega}}$. Furthermore, the velocity of the incoming wave in the normal direction is given by

$$\begin{aligned}\frac{d}{dt}(\mathbf{n}\cdot\nabla\phi_I)&=\mathbf{n}\cdot\frac{d}{dt}(\nabla\phi_I)+\nabla\phi_I\cdot\frac{d\mathbf{n}}{dt}\\&=\mathbf{n}\cdot\left(\frac{\partial\nabla\phi_I}{\partial t}+((\mathbf{u}+\boldsymbol{\omega}\times\mathbf{r})\cdot\nabla)\nabla\phi_I\right)-\mathbf{n}\cdot(\boldsymbol{\omega}\times\nabla\phi_I)\end{aligned} \tag{19}$$

Finally, combining the results from Eqs. (16), (18) and (19) and substituting these with the time derivative of the body boundary condition given in Eq. (10) leads to the following condition for the potential function φ

$$\frac{\partial\varphi}{\partial n}=\mathbf{n}\cdot\left[(\dot{\mathbf{u}}+\dot{\boldsymbol{\omega}}\times\mathbf{r})-(\boldsymbol{\omega}\times\mathbf{u})\right]-\mathbf{n}\cdot\left[\frac{\partial\nabla\phi_I}{\partial t}+((\mathbf{u}+\boldsymbol{\omega}\times\mathbf{r})\cdot\nabla)\nabla\phi_I-(\boldsymbol{\omega}\times\nabla\phi_I)\right]. \tag{20}$$

this is the body boundary condition for the potential function φ on the body surface $S_B(t)$. Once the potential function φ and the velocity potential ϕ are known, the time derivative of the velocity potential ϕ_t is given by

$$\phi_t=\frac{\partial\phi}{\partial t}=\varphi-\mathbf{U}\cdot\nabla\phi. \tag{21}$$

the function φ can be solved using the same source formulation that is used to solve the perturbation velocity potential ϕ. The potential function φ is based on the same solution as the velocity potential ϕ, except that it satisfies different boundary conditions on the body surface S_B. The potential function φ satisfies the linear free surface boundary condition and Laplace's equation. Furthermore, the radiation and bottom boundary conditions are satisfied by the transient Green function that is used to solve the potential function φ. The initial conditions at $t=0$ are the same for the potential function φ and for the perturbation velocity potential ϕ.

The boundary condition for the potential function φ was derived applying the absolute time derivative of the fluid and the body velocities given in the normal direction on the point of the body surface. Hence, the first term inside the square brackets on the right-hand side of the condition (20) does not give the acceleration of the point on the body surface (term $\dot{\mathbf{u}}+\dot{\boldsymbol{\omega}}\times r-\boldsymbol{\omega}\times\mathbf{u}$). The term $\varphi-\mathbf{U}\cdot\nabla\phi$ can be regarded as the rate of change of ϕ in the moving coordinate system, i.e. the rate of change of ϕ at a fixed point of fluid measuring from a moving body of which the velocity is $\mathbf{U}$ (Milne-Thomson, 1968, p. 89, 3–61). If the body is in constant translational motion, then the body acceleration is zero and the first term on the right-hand side in (20) is zero. Furthermore, if the body is in constant translational motion in calm water then the right-hand side is entirely zero. Hence, the potential function φ is also zero. Then, the Bernoulli's equation includes only the term $-\mathbf{U}\cdot\nabla\phi$ from the acceleration potential ϕ_t. From this it also follows that if the body is in steady motion, the term $\phi_t=\partial\phi/\partial t=$is not zero in a space-fixed coordinate system (Batchelor, 1967, p. 404). If the body is translating at a constant forward velocity U_0 in calm water and the other motions are zero then the term gives $\varphi-\mathbf{U}\cdot\nabla\phi=-U_0\partial\phi/\partial x$.

The higher order derivatives of ϕ do not appear in the boundary condition (20) because the potential function φ is used. The direct solution of the ϕ_t term includes second-order derivatives of ϕ with respect to the space variables; $(\mathbf{n}\cdot\nabla)\nabla\phi$ (Wu, 1998; Bandyk and Beck, 2011). The indirect solution applied to the present time domain method saves computational time because the evaluation of the higher order derivatives of the transient Green function is not needed.

The body accelerations appear on the right-hand side of the boundary condition for the potential function φ in Eq. (20). However, equations of motion have not yet been solved that give the accelerations for the freely floating body, i.e. the body accelerations are unknown. The acceleration potential exists in Bernoulli's equation that is used to determine the forces and moments on the body. The forces and moments are needed in the equations of motion, and the accelerations are not known until the equations of motion are solved. In the present time domain method, an iterative solution procedure is applied to solve the accelerations and the function φ. Another technique is to combine the boundary value problem of the acceleration potential and the equations of motion to solve the acceleration of the body directly (Wu and Eatock Taylor, 1996; Bandyk and Beck, 2011).

2.3. Velocity and acceleration potentials

The solutions of the perturbation velocity and acceleration potentials are obtained from integral equations by applying Green's theorem. The potentials are expressed with source distributions over the body, where the source distributions are represented by a transient Green function. In the numerical solution, the body surface is discretised by panels and the velocity and acceleration potentials are determined using the constant panel method. The transient Green function can be decomposed into the impulsive and memory parts as follows:

$$G=G^{(0)}+G^{(t)} \tag{22}$$

The impulsive part is given as

$$G^{(0)}=\frac{1}{R}-\frac{1}{R'}, \tag{23}$$

where $R=\sqrt{(x-x')^2+(y-y')^2+(z-z')^2}$, $R'=\sqrt{(x-x')^2+(y-y')^2+(z+z')^2}$. The field point P is at the point (x, y, z), and the source point Q is at (x',y',z'). The image source Q' is located at the point $(x',y',-z')$. The memory part is (Wehausen and Laitone, 1960, p. 491, Eq. (13.49))

$$G^{(t)}=2\int_0^\infty\left[e^{k(z+z')}\sqrt{gk}\ \sin(\sqrt{gk}(t-\tau))J_0(kr)\right]dk, \tag{24}$$

where $r=\sqrt{(x-x')^2+(y-y')^2}$ and J_0 is the Bessel function of the first kind of order zero. The present time is t and the time delay $t-\tau$ gives the memory effect at time t of the fluid flow at time τ. In numerical computations, the series expansion can be used to solve the memory part (see for example Newman, 1992). By applying the series and asymptotic expansions, the solution domain is divided into sub-domains in which the different solution schemes are applied (Liapis and Beck, 1985). Polynomial approximations and Filon's integral formulae have been used in addition to the series and asymptotic expansions (Lin and Yue, 1991; Sen, 2002). In the present calculation method, the memory part of the transient Green function and its derivatives are solved beforehand with the use of a numerical integration (Kukkanen, 2012). During the calculation in the time domain, the values of the memory part are interpolated from the pre-calculated results using the finite element presentation of the memory part of the Green function. The interpolation is based on the finite element shape functions, and nine-node quadrilateral elements are used to describe the shape functions.

The velocity potential ϕ and the Green function G can be expressed by means of Green's theorem. This derivation for the integral equation is given by Lin and Yue (1991), and Ferrant (1991). The integral equation for the velocity potential using the distribution of sources can be written as follows:

$$\begin{aligned}\varphi(P,t)=&\frac{1}{4\pi}\iint_{S_B(t)}\sigma(Q,t)\,G^{(0)}(P,Q)dS\\&+\frac{1}{4\pi}\int_0^t\left[\iint_{S_B(\tau)}\sigma(Q,\tau)\,G^{(t)}(P,Q,t,\tau)dS\right]d\tau\\&-\frac{1}{4\pi}\frac{1}{g}\int_0^t\left[\int_{\Gamma_F(\tau)}\sigma(Q,\tau)\,G^{(t)}(P,Q,t,\tau)\,u_nU_N d\Gamma\right]d\tau,\end{aligned} \tag{25}$$

where the source strength is σ. The velocity $u_n=\mathbf{u}\cdot\mathbf{n}$ is the velocity of the body in the normal direction at the intersection of the body and the free surface at source point Q at time τ. The surface and line integrals, $S_B(\tau)$ and $\Gamma_F(\tau)$ and the derivative in the normal direction are expressed in the source point coordinates

Q at (x',y',z'). The source and field points P and Q depend on time t in the body nonlinear solution because the body position is updated during the calculation. The line integral $\Gamma_F(\tau)$ is evaluated at the intersection of the body and the free surface. The velocity $U_N=\mathbf{U}_\Gamma\cdot\mathbf{N}$ is the two-dimensional velocity of Γ_F in the normal direction $\mathbf{N}=\mathbf{N}(Q,\tau)$ where $\mathbf{N}$ is the normal vector of Γ_F at $z=0$.

In the above integral equation, the source strengths are unknown at time t. The unknown source strengths can be solved using the condition of the velocities of the fluid and body on the body surface, i.e. the body boundary condition (4). The body boundary condition is $\partial\phi/\partial n=\mathbf{n}\cdot\nabla\phi=(\mathbf{U}\cdot\mathbf{n}-\partial\phi_I/\partial n)$. Thus, the unknown source strengths of the velocity potential can be solved from the following equation:

$$\begin{aligned}&\frac{1}{4\pi}\iint_{S_B(t)}\sigma(Q,t)\frac{\partial G^{(0)}(P,Q)}{\partial n}dS=-\left(\mathbf{U}\cdot\mathbf{n}-\frac{\partial\varphi_I}{\partial n}\right)\\&+\frac{1}{4\pi}\int_0^t\left[\iint_{S_B(\tau)}\sigma(Q,\tau)\frac{\partial G^{(t)}(P,Q,t,\tau)}{\partial n}dS\right]d\tau\\&-\frac{1}{4\pi}\frac{1}{g}\int_0^t\left[\int_{\Gamma_F(\tau)}\sigma(Q,\tau)\frac{\partial G^{(t)}(P,Q,t,\tau)}{\partial n}u_nU_N d\Gamma\right]d\tau,\end{aligned}\tag{26}$$

where the normal derivative $\partial/\partial n=\mathbf{n}\cdot\nabla$ is given with respect to the field point coordinates (x, y, z). Once the source strengths are known, the velocity potential can be determined from Eq. (25). In the acceleration potential method, the above equations are also valid for the potential function φ, replacing ϕ with φ. In solving the source strengths for the potential function φ, the condition $\partial\varphi/\partial n=\mathbf{n}\cdot\nabla\varphi$ for the acceleration potential is applied. Hence, the condition $(\mathbf{U}\cdot\mathbf{n}-\partial\phi_I/\partial n)$ in the above Eq. (26) is replaced by the condition given by the right-hand side of Eq. (20). Thus, applying Eq. (26) the source strengths for the potential function ϕ can be solved and then the potential function ϕ can be expressed with a similar equation to Eq. (25). The time derivative of the velocity potential is finally given by Eq. (21).

2.4. Pressure loads and equations of motion

The pressure on the body can be determined from Bernoulli's equation

$$p_1(P,t)=-\rho\left[\frac{\partial\Phi}{\partial t}+\frac{1}{2}|\nabla\Phi|^2+gz\right],\tag{27}$$

where the velocity potential is the combination of the perturbation and incoming wave velocity potentials $\Phi=\phi+\phi_I$. Using $\phi+\phi_I$ and the acceleration-potential solution for ϕ_t given by Eq. (21), Bernoulli's equation can be written in the following form:

$$p_1(P,t)=-\rho\left[\varphi-\mathbf{U}\cdot\nabla\phi+\frac{1}{2}|\nabla\phi|^2+\frac{\partial\phi_I}{\partial t}+\frac{1}{2}|\nabla\phi_I|^2+\nabla\phi\,\nabla\phi_I+gz\right].\tag{28}$$

Forces and moments on the body are obtained by integrating the pressure over the wetted surface of the body. The forces $\mathbf{F}=(F_1, F_2, F_3)$ and moments $\mathbf{M}=(F_4, F_5, F_6)$ can be determined as follows

$$F_i(t)=\int_{S_B(t)}p_1(P_0,t)n_{0\,i}dS,\quad i=1,2,\ldots,6,\tag{29}$$

where n_{0i} are components of the normal vectors. The normal vector for the forces is given as

$$\mathbf{n}=n_{0\,1}\mathbf{i}+n_{0\,2}\mathbf{j}+n_{0\,3}\mathbf{k},\tag{30}$$

and the generalised normal vector for the moments is defined as follows:

$$\mathbf{r}\times\mathbf{n}=n_{0\,4}\mathbf{i}+n_{0\,5}\mathbf{j}+n_{0\,6}\mathbf{k}.\tag{31}$$

The position vector from the centre of gravity of the body indicating point P_0 on the body surface is $\mathbf{r}=x_0\mathbf{i}+y_0\mathbf{j}+z_0\mathbf{k}$. Point P_0 is given in the body-fixed coordinate system at (x_0, y_0, z_0). In addition, the vector components in $\mathbf{n}$ and $\mathbf{r}\times\mathbf{n}$ are expressed in the body-fixed coordinate system. Thus, the forces and moments are expressed in the body-fixed coordinate system. The forces and moments are expressed in the body-fixed coordinate system because the equations of motion given in the coordinate system are fixed on the body and the origin is at the centre of gravity. The accelerations of the body are solved by the equations of motion:

$$\begin{aligned}&m(\dot u+qw-rv)=F_1+F_{G1}\\&m(\dot v+ru-pw)=F_2+F_{G2}\\&m(\dot w+pv-qu)=F_3+F_{G3}\\&I_{44}\dot p+I_{45}\dot q+I_{46}\dot r+(I_{66}-I_{55})\,qr-I_{45}rp+I_{64}pq+I_{56}(q^2-r^2)=F_4\\&I_{54}\dot p+I_{55}\dot q+I_{56}\dot r+(I_{44}-I_{66})\,rp-I_{56}pq+I_{45}qr+I_{64}(r^2-p^2)=F_5\\&I_{64}\dot p+I_{65}\dot q+I_{66}\dot r+(I_{55}-I_{44})\,pq-I_{64}rq+I_{56}rp+I_{45}(p^2-q^2)=F_6\end{aligned}\tag{32}$$

here, m is the mass of the body and I_{ij} are the mass moment of inertias of the body with respect to the body-fixed coordinate system. The translational velocity components in the body-fixed coordinate system are u, v and w in the x_0-, y_0- and z_0-directions, respectively. The angular velocities in the body-fixed coordinate system are p, q and r about the x_0, y_0 and z_0 axis, respectively. The components of the gravity force F_{Gi} in the body-fixed coordinate system are given by

$$\mathbf{F}_G=(F_{G1},\,F_{G2},\,F_{G3})=mg(\sin\,\eta_5,-\,\sin\,\eta_4\,\cos\,\eta_5,-\,\cos\,\eta_4\,\cos\,\eta_5)\tag{33}$$

The translational and angular velocities are transformed to the space-fixed coordinate system using the transformation matrices. The relations between the body and space-fixed coordinate systems are given by the Eulerian angles roll, pitch and yaw. The orientation of the body velocities from the body-fixed coordinate system to the space-fixed coordinate system is obtained using the following transformation matrices:

$$\dot{\mathbf{x}}_G=[\mathbf{L}]\,\mathbf{u}\tag{34}$$

$$\boldsymbol{\Omega}=[\mathbf{B}]\,\boldsymbol{\omega}\tag{35}$$

here, $\mathbf{u}=(u, v, w)$ is the vector of translational velocities and $\boldsymbol{\omega}=(p, q, r)$ is the vector of the angular velocities expressed in the body-fixed coordinate system. In the space-fixed coordinate system, the same velocities are the translational velocities $\dot{\mathbf{x}}_G=(\dot\eta_1,\,\dot\eta_2,\,\dot\eta_3)$ and the rotational velocities $\boldsymbol{\Omega}=(\dot\eta_4,\,\dot\eta_5,\,\dot\eta_6)$. The transformation matrix is $[\mathbf{L}]$ for the translational velocities and $[\mathbf{B}]$ for the angular velocities. The matrices are given as follows:

$$[\mathbf{L}]=\begin{bmatrix}c5c6 & -c4s6+s4s5c6 & s4s6+c4s5c6\\ c5s6 & c4c6+s4s5s6 & -s4c6+c4s5s6\\ -s5 & s4c5 & c4c5\end{bmatrix}\tag{36}$$

$$[\mathbf{B}]=\begin{bmatrix}1 & s4t5 & c4t5\\ 0 & c4 & -s4\\ 0 & s4/c5 & c4/c5\end{bmatrix}\tag{37}$$

where $ci=\cos\eta_i$, $si=\sin\eta_i$ and $t5=\tan\eta_5$. The transformation matrix $[\mathbf{L}]$ is also used to transform directional vectors between the body-fixed and space-fixed coordinate systems. The transformation matrices

are applied to perform all the vector operations in the same coordinate system.

In the body linear solution, the body position is not updated during the calculation and the wetted surface of the body is the same as at $t=0$ for all $t>0$. The pressure is solved for the mean wetted surface below the mean water level $z=0$. In the body nonlinear solution, the instantaneous position of the body is updated during the calculation. The pressure is solved for the instantaneous, wetted surface of the body below $z=0$. At every time step, all of the panels are checked to find out if they are above or below the free surface level. The panel is considered wet if all of the corner points of the panel are below the water level, $z=0$. Otherwise, the panel is dry and then it is not included in the solution. The line integral at the waterline is approximated at the centroid of the panels.

In addition to the body linear and nonlinear solutions, the time domain method includes the option to solve forces and moments using what is termed a body-wave nonlinear solution. The body-wave nonlinear solution is the same as the body nonlinear solution but additional nonlinear effects are included with the Froude–Krylov and hydrostatic restoring forces and moments. The Froude–Krylov and hydrostatic restoring pressures are solved up to the free surface elevation of the incoming wave.

The rigid hull girder loads are the normal force (V_1), lateral shear force (V_2), vertical shear force (V_3), torsion moment (V_4), vertical bending moment (V_5) and lateral bending moment (V_6). The hull girder loads are determined in the body-fixed coordinate system. The positive direction of the forces (V_1, V_2, V_3) is the same as that of the axis of the body-fixed coordinate system. The moments (V_4, V_5, V_6) are defined about the axis in the body-fixed coordinate system. The internal hull girder loads at cross section x_p of the body can be determined as follows:

$$V_i(t,x_p)=\int_{V(x_p)} a_{m\,i}\,dm-\int_{S_B(x_p)} p_1 n_{p\,i}\,dS,\quad i=1,2,\ldots,6, \tag{38}$$

where a_{mi} are the acceleration components of the mass dm. The integrations are carried out from the stern of the body to the cross section x_p. For the hydrodynamic forces and moments, the integration includes the wetted surface of the body $S_B(x_p)$ to a cross section at x_p. For the inertia forces and the moment of inertia terms, the integration is performed over the volume $V(x_p)$ of the mass distribution of the body from the stern to a cross section at x_p. In the equation presented above, n_{pi} are the components of the generalised normal vectors for the forces and moments.

3. Results

3.1. Wigley

The comparison of the time domain calculation method with the model test results are given for the Wigley III hull form, for which the model test results are presented by Journee (1992). The panel mesh of the hull used in the calculation is shown in Fig. 2. All of the results presented here were calculated in head waves. At time $t=0$, the wave amplitude was a, the forward speed was U_0 and the other motions were zero. The results were calculated using the acceleration potential method to solve the time derivative of the velocity potential in Bernoulli's equation.

Time histories of the heave calculated with different panel meshes are shown in Fig. 3. Half of the hull was discretised by 180, 320 and 500 quadrilateral panels. The wave frequency was $\omega\sqrt{L/g}=2.24$ and the forward speed given by the Froude number was $Fn=0.30$ ($Fn=U_0/\sqrt{gL}$). In the calculations, the number of time steps in one period was $T_e/\Delta t=46$, where T_e was the encounter wave period. The calculation results are based on the

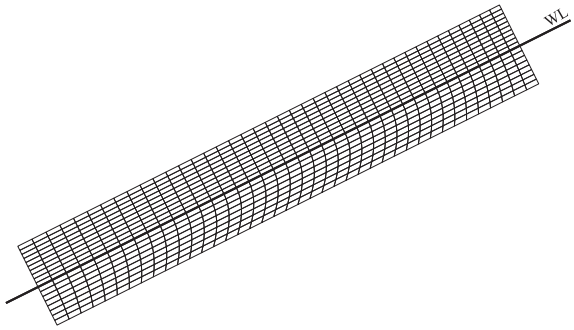

Fig. 2. The panel mesh of the Wigley III hull form. The number of panels on the half hull below the still waterline (WL) is 320.

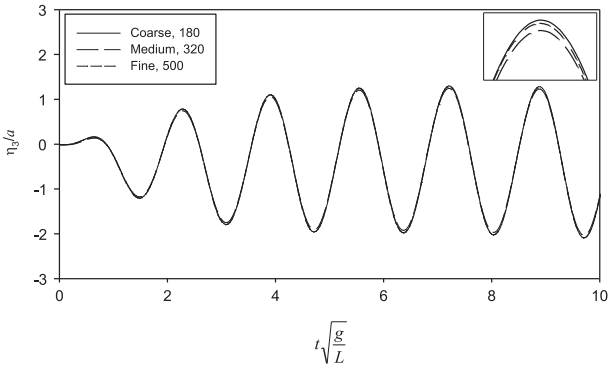

Fig. 3. Time history of heave at forward speed $Fn=0.30$ in head waves at wave frequency $\omega\sqrt{L/g}=2.24$. The number of panels was 180, 320 and 500 on the half hull.

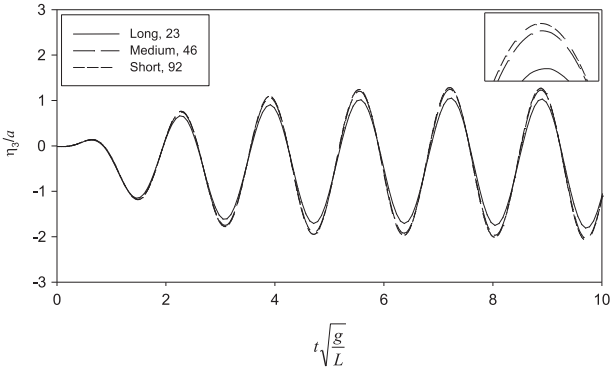

Fig. 4. Time history of heave at forward speed $Fn=0.30$ in head waves at wave frequency $\omega\sqrt{L/g}=2.24$. The number of time steps in one period was $T_e/\Delta t=23$, 46 and 92. The number of panels was 320 on the half hull.

body linear solution. The figure shows that the different mesh sizes have an effect on the convergence of the solution for the heave amplitudes and the amplitudes fluctuate somewhat between the coarse and fine meshes. However, the difference in the amplitudes of the heave is less than 3% between the different meshes. In the rest of the calculations, the number of panels was 320 on half of the Wigley III hull form.

The calculation results using three different time step sizes are presented in Fig. 4. The calculations were performed using the number of time steps in one encounter period $T_e/\Delta t=23$, 46 and 92. The calculated time histories of the heave are based on the

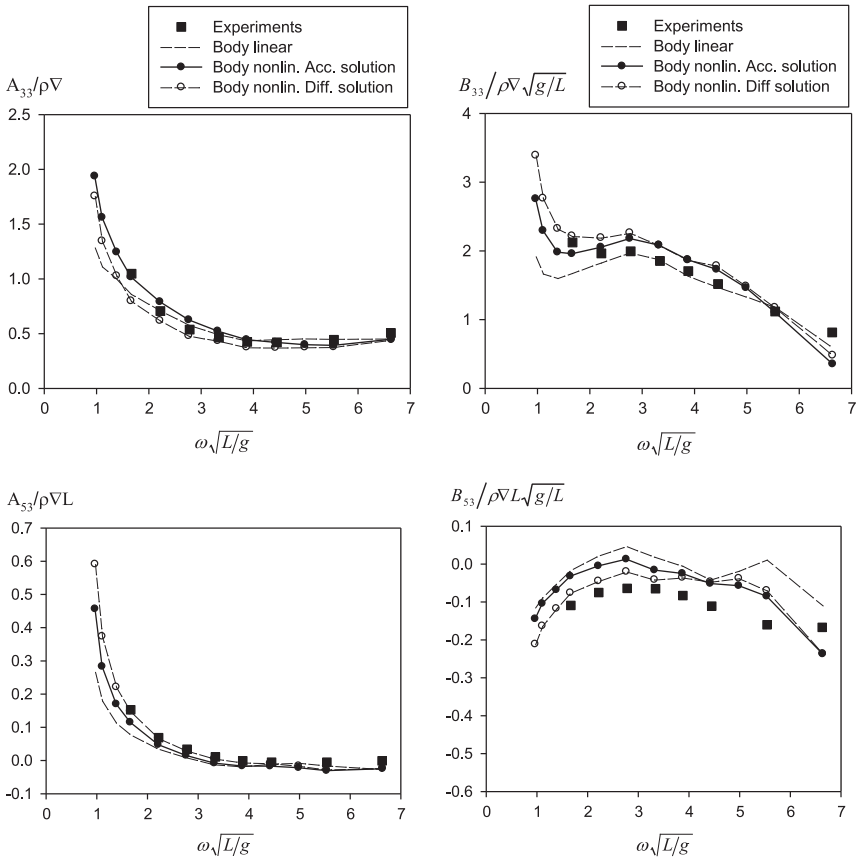

Fig. 5. Heave and pitch added mass and damping coefficients in heave at $Fn=0.3$. The experimental results are from Journee (1992).

body linear solution. The wave frequency was $\omega\sqrt{L/g}=2.24$ and the forward speed $Fn=0.30$. The number of time steps $T_e/\Delta t=46$ gives 2% lower heave amplitudes than the shortest time step size for which the number of time steps in one period is $T_e/\Delta t=92$. However, the difference between the longest and shortest time step sizes is 15%. The longest time step size gives lower motion amplitudes than the shorter time step sizes. In the rest of the calculations to determine the body motions, forces and moments for the Wigley III hull form, the number of time steps in one encounter period was about 50.

The added mass and damping coefficients at forward speed were determined from the forced oscillation in the calm water. The body was oscillating harmonically at the given heave or pitch amplitude and frequency. The oscillation amplitude was 0.025 m and 1.5 degrees in heave and pitch, respectively, which were the same as in the model tests. The time histories of the radiation forces and moments in heave and pitch were calculated and Fourier transforms were performed to define the added mass and damping coefficients. The added mass corresponds to the in-phase component with the body acceleration of the radiation force or moment, and the damping corresponds to the in-phase component with the velocity. The heave and pitch added mass and the damping coefficients in heave are shown in Fig. 5 and in pitch in Fig. 6 at the Froude number $Fn=0.3$. The body linear and nonlinear solutions for the added mass and damping coefficients are given in the figures. The acceleration potential method was used to solve the time derivative of the velocity potential determining the added mass and damping coefficients. In addition to the acceleration potential method, the backward difference method was also used in the body nonlinear solution. The acceleration potential and backward difference methods give similar predictions for the added mass and damping coefficients. In the acceleration potential solution, the time derivative of the velocity potential was calculated accurately at each time step because the body was in forced monochromatic oscillation and hence the body motions, velocities and accelerations were known at each time step. However, the time derivative of the velocity potential was solved numerically in the backward difference method. Hence, these two methods resulted in slightly different time histories which were used to determine the added mass and damping coefficients. Furthermore, the body linear and nonlinear solutions are close to each other. The diagonal coefficients, A_{ii} and B_{ii}, are in good agreement with the experiments. Moreover, the predictions for the cross-coupling added mass coefficients are satisfactory, but larger differences exist in the cross-coupling damping terms. For the pitch added mass and damping coefficients, the body nonlinear solution gives better results than the body linear solution. In the body nonlinear solution, the forward speed effects are taken into account at the instantaneous floating position. Hence, the angle of attack due to pitch in the steady flow is determined for the actual body geometry below the mean water level.

The transfer functions of the heave and pitch at forward speed $Fn=0.30$ in head waves are shown in Fig. 7. In the calculations, the wave amplitude was $a/L=0.0067$. Calculations were carried out using the body linear and nonlinear solutions. In general, the calculated motions are in close agreement with the model test results. At the heave resonance, the calculation overestimates the heave motion. At the longer waves, the body nonlinear solution gives somewhat larger amplitudes for the heave motion than the body linear solution. Both the body linear and nonlinear methods

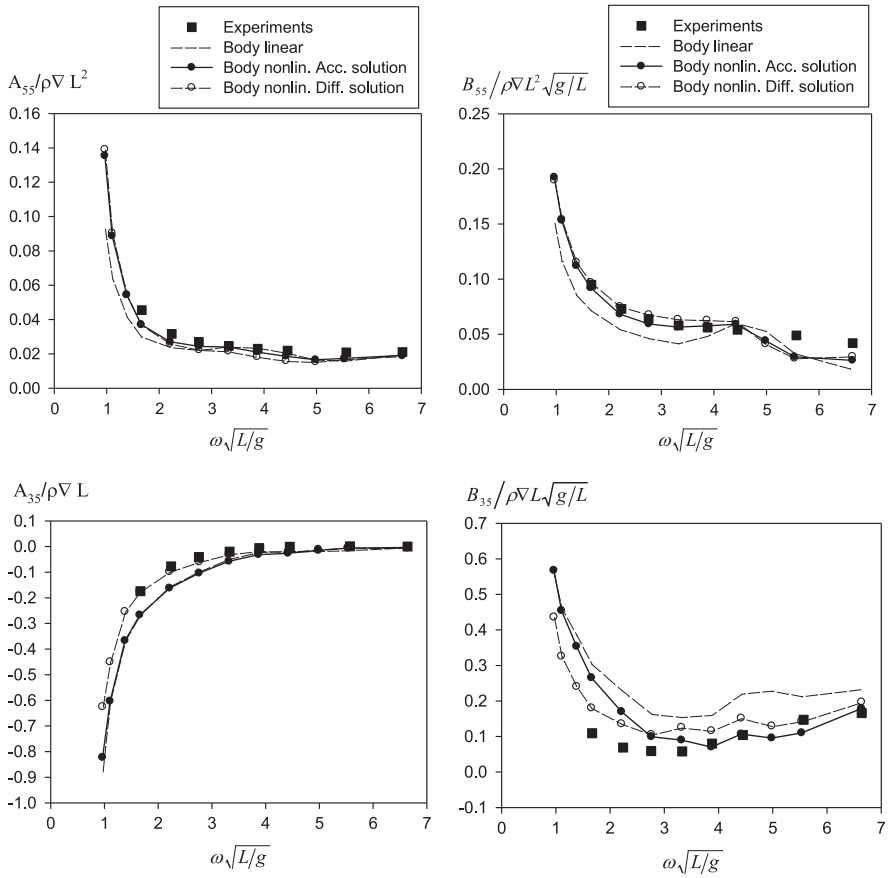

Fig. 6. Heave and pitch added mass and damping coefficients in pitch at $Fn=0.3$. The experimental results are from Journee (1992).

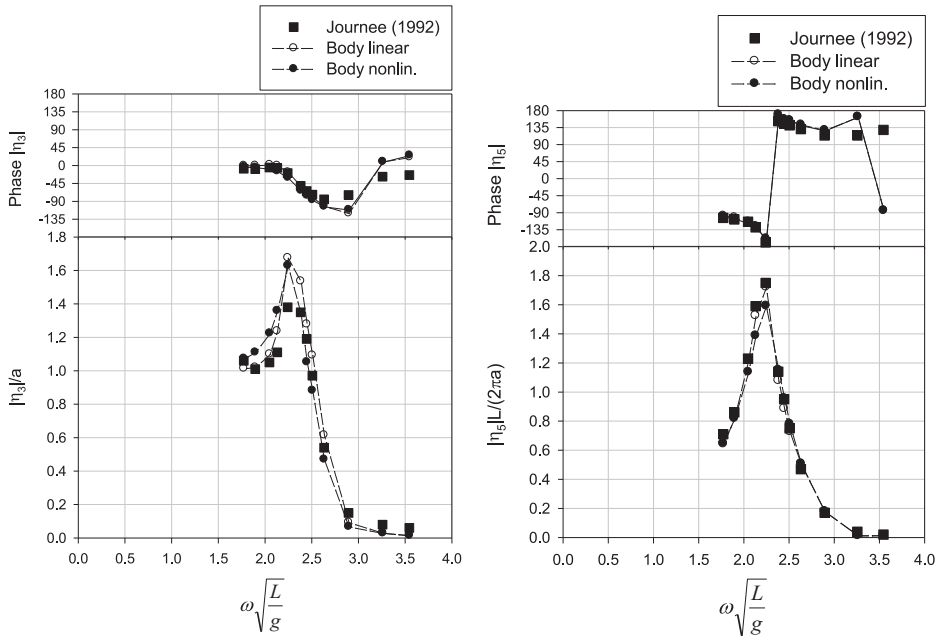

Fig. 7. Heave and pitch of the Wigley III in head waves at $Fn=0.30$.

give close to the same results at the heave resonance. Hence, the nonlinearities due to the instantaneous position of the body with respect to the still water level cannot explain the differences with the model test results. In the governing equations, it is assumed that the free surface boundary condition is linear and the flow is inviscid. These assumptions can possibly have an effect on the

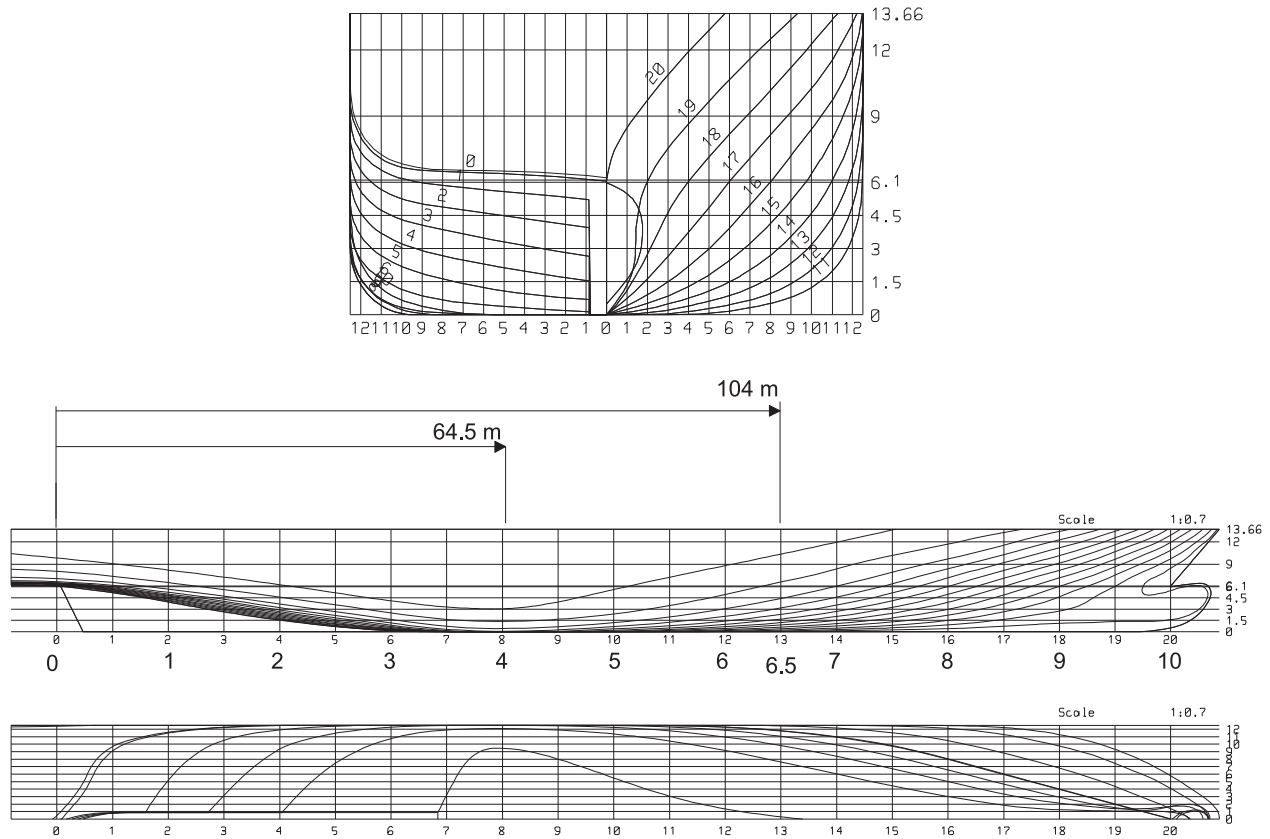

Fig. 8. Lines drawing of the RoPax ship. The longitudinal locations of the force transducers are measured from the AP (frame 0). The midship transducer was located at frame 4 and the foreship transducer at frame 6.5.

Table 1
Main dimensions and weight data of the RoPax ship. The aft perpendicular is AP at lines drawing frame 0, CL is the centre line and BL is the base line.

Quantity	Symbol	Unit	Value
Length overall	L_{oa}	[m]	171.4
Length between perpendiculars	L_{pp}	[m]	158.0
Breadth max. at waterline	B_{wl}	[m]	25.0
Draught	T	[m]	6.1
Displacement	∇	[m^3]	13 766
Block coefficient	C_B	–	0.55
Centre of gravity:			
From AP	x_{CG}	[m]	74.9
From CL	y_{CG}	[m]	0.0
From BL	z_{CG}	[m]	10.9
Radius of gyration in pitch	k_{yy}/L_{pp}	–	0.25

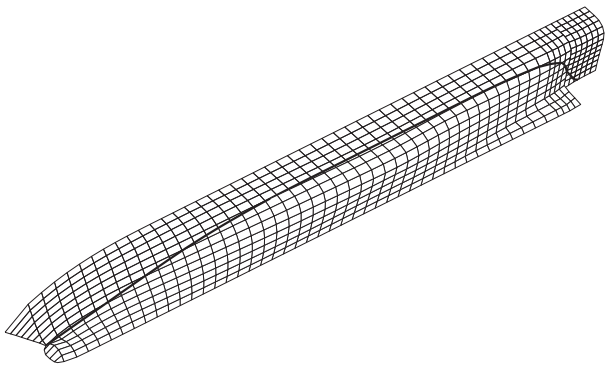

Fig. 9. Panel meshes of the RoPax ship in the calculations. The number of panels is 327 on the half body below the still waterline.

calculated results. The body linear and nonlinear solutions give good predictions for the pitch. However, the body nonlinear solution gives slightly lower amplitudes near the resonance of the pitch.

3.2. RoPax ship

Model tests were carried out for the RoPax ship to investigate the hull girder loads in regular and irregular head waves and also in calm water (Kukkanen, 2012). The ship has a bulbous bow and a flat-bottom stern at the waterline. The lines drawing is shown in Fig. 8 and the main dimensions and weight data used in the model tests are given in Table 1. The ship model was manufactured to a scale of 1:39.024. The ship model was a segmented ship model and force and moment transducers were installed in two cut-off sections. The locations of the force and moment transducers are shown in Fig. 8. The midship transducer was at frame 4 ($x/L=0.40$) and the foreship transducer at frame 6.5 ($x/L=0.65$). The characteristic length L of the ship is the length between the perpendiculars L_{pp}. The transducers were installed at the centre line and the vertical distance from the base line was the same as the centre of gravity of the ship. According to the calibration certificate of the force transducers, the measurement uncertainties were 4.25% and 3.25% for the shear force and bending moment, respectively. The heave and pitch motions were measured at the centre of gravity of the ship model.

The panel meshes of the RoPax ship are shown in Fig. 9. The number of panels on the half hull below the still waterline was 327. The transom of the ship was not included on the panel mesh.

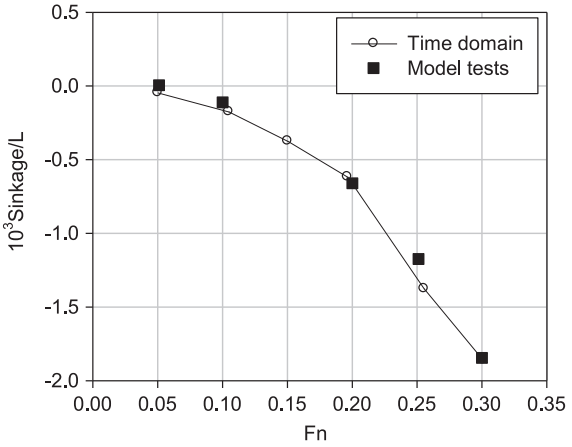

Fig. 10. Sinkage positive upwards at the centre of gravity of the ship in calm water as a function of the ship speed.

Hence, the transom was always dry and the pressure was the same as the atmospheric pressure at the transom. The time step used in the calculation was $\Delta t\sqrt{g/L}=0.025$.

Responses in calm water were also measured in the calm water and compared to those of the calculated results. The body nonlinear solution was used in the calculation. The sinkage at the centre of gravity of the ship is shown in Fig. 10 as a function of the ship speed. The vertical shear force at foreship and the vertical bending moment at midship are presented in Fig. 11. The calculated sinkage, shear force and bending moment are similar to those in the model tests. The vertical bending moment increases with the speed. The steady pressure and wave pattern due to the forward speed induce a sagging bending moment on the hull girder.

The linear transfer functions are presented in Figs. 12–15. In the time domain calculation, the wave amplitude related to the ship length was $a/L=0.006$ in regular waves in order to determine the first harmonic component of the response. The first harmonic component gives the linear transfer function for the response. The model test results are presented for wave amplitudes $a/L=0.006$, 0.013 and 0.019 at zero speed and $a/L=0.006$ and 0.013 at forward speed $Fn=0.25$. The first harmonic components from the model tests were close to each other at the different wave amplitudes. Hence, the nonlinearities are relatively small in the first harmonic components

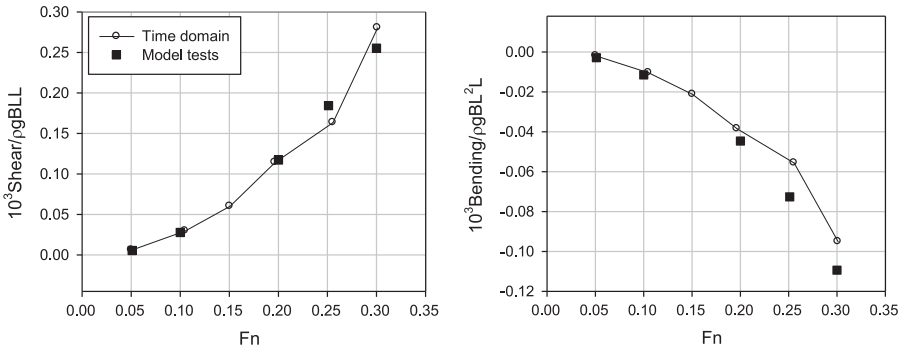

Fig. 11. Shear force at the foreship (left) and vertical bending moment at midship (right) in calm water as a function of the ship speed.

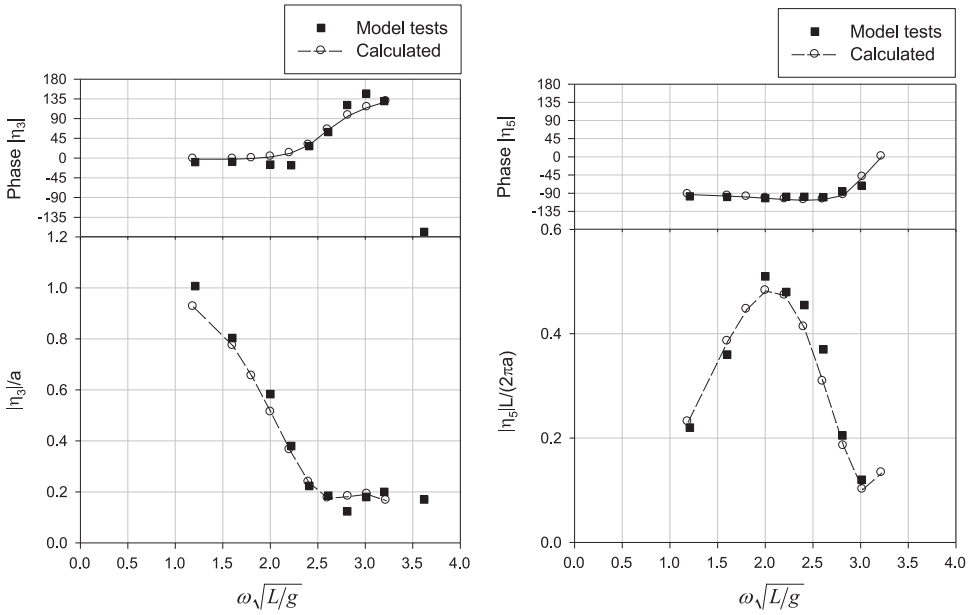

Fig. 12. Heave and pitch at $Fn=0.0$ in head seas calculated with the body-wave nonlinear solution.

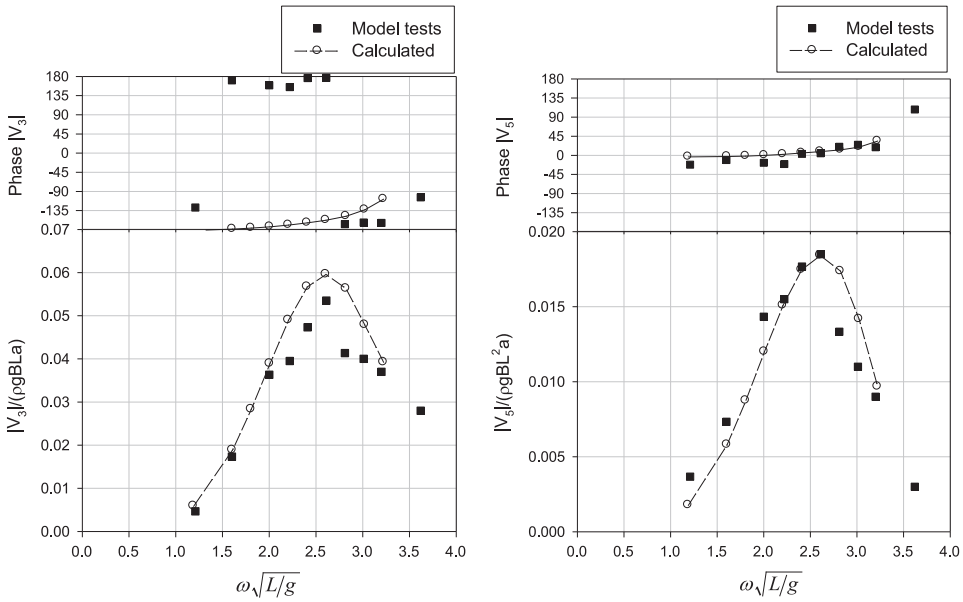

Fig. 13. Shear force at the foreship and bending moment at midship at $Fn=0.0$ in head seas calculated with the body-wave nonlinear solution.

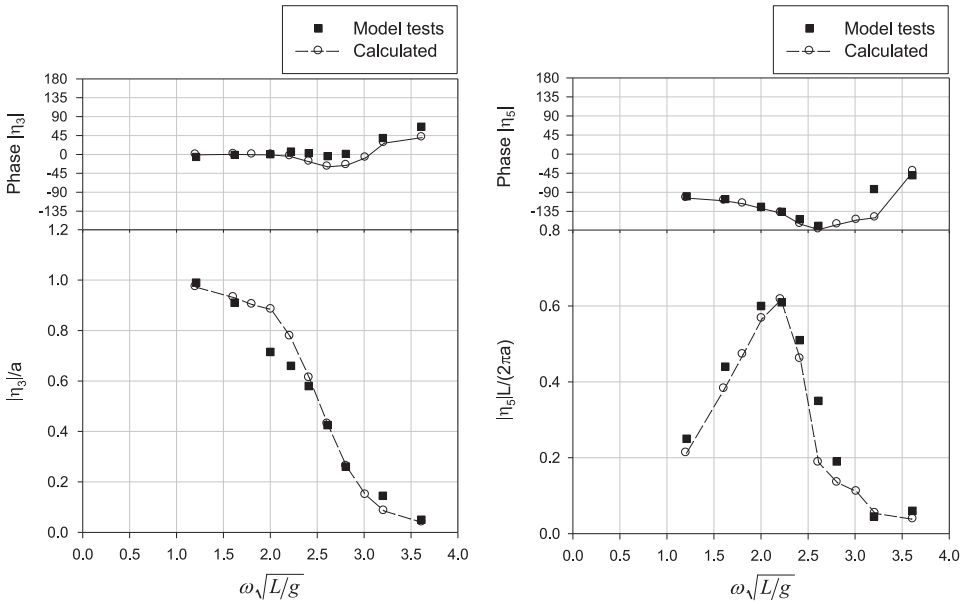

Fig. 14. Heave and pitch at $Fn=0.25$ in head seas calculated with the body-wave nonlinear solution.

of the responses with respect to the first harmonic component of the wave amplitude. However, the mean of the response and the single positive and negative amplitudes, i.e. the higher order components, are not necessarily linear with respect to wave amplitude.

At zero speed, the transfer functions for heave and pitch are presented in Fig. 12 and for the shear force and bending moment in Fig. 13. The results using the time domain calculation method are based on the body-wave nonlinear solutions. The calculated results are in good agreement with the model test results. The time domain method gives a slightly higher prediction for the shear force and bending moment. At forward speed $Fn=0.25$, the transfer functions are shown in Fig. 14 for the heave and pitch and for the shear force and bending moment in Fig. 15. The body-wave nonlinear solution and the model test results of the shear force and bending moment are close to each other at forward speed $Fn=0.25$. The transfer function of the calculated shear force exists at somewhat lower wave frequencies than in the model tests. The pitch motion is also close to the model test results, but the calculation gives rather high heave amplitude at the resonance.

The maximum and minimum peaks of the bending moment in regular head waves and the contribution of the steady bending moment at forward speed $Fn=0.25$ are presented in Fig. 16. The figure is given in a dimensional form in order to gain an insight into the contribution of the steady bending moment to the sagging and hogging bending moment. The maximum and minimum peaks are given for two wave amplitudes, $a/L=0.006$ and 0.013

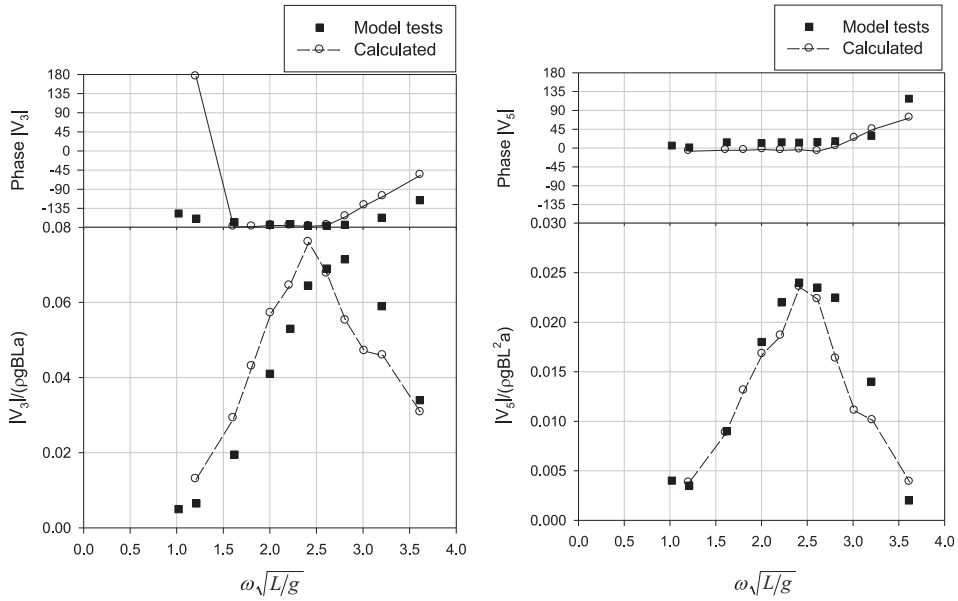

Fig. 15. Shear force at the foreship and bending moment at midship at $Fn=0.25$ in head seas calculated with the body-wave nonlinear solution.

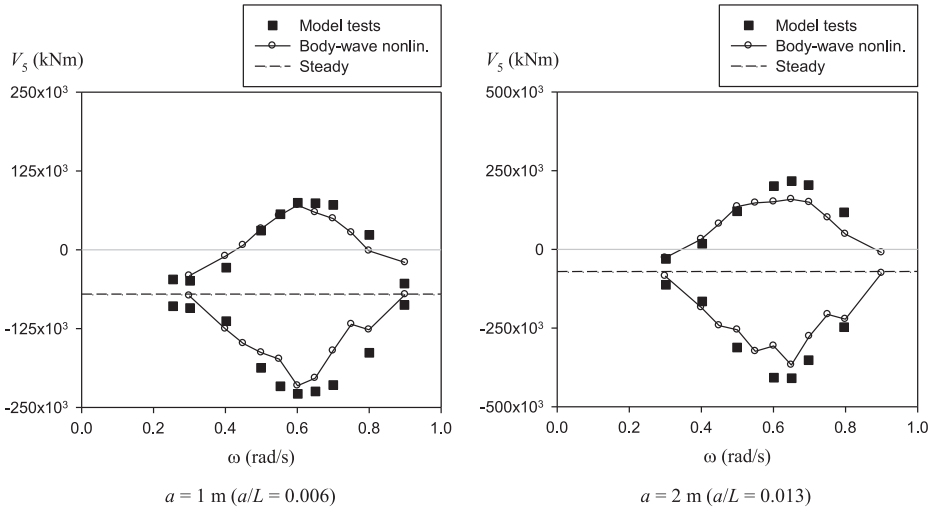

Fig. 16. Maximum and minimum peaks of the bending moment in regular waves and the contribution of the steady bending moment at $Fn=0.25$. The calculation was carried out using the body-wave nonlinear solution. The given steady bending moment is based on the model test results.

($a=1$ m and 2 m). It can be noted that the mean of the maximum and minimum at the longest and shortest waves is about the same as the steady bending moment in calm water with the forward speed. The contribution of the steady bending moment also explains a large part of the differences between the sagging and hogging bending moment at the lower wave amplitude. However, the contribution of the steady bending moment is small at the higher wave amplitude. At higher wave amplitudes, the steady bending moment is small and a large part of the nonlinearities in sagging and hogging is due to the ship motions in waves.

In irregular waves, calculated responses are compared with the model test results at zero speed. The significant wave height was $H_s=9$ m and the zero crossing period was $T_z=10.5$ s in the model tests and calculations. The irregular waves were generated using the modified Pierson–Moskowitz wave spectrum (ITTC, 2002). The irregular long-crested waves were described as a sum of regular wave components with different amplitudes and phases. The time history of the irregular wave was generated in the same way in the model tests and calculations. The duration of the

Table 2
Mean and standard deviation (St.Dev.) of responses in sea state $H_s=9.0$ m and $T_z=10.5$ s at $Fn=0.0$.

		Time domain		Model tests	
		Mean $\bar{x}$	St.dev. σ_x	Mean $\bar{x}$	St.dev. σ_x
Wave	a/H_s	0.000	0.246	−0.003	0.251
Heave	η_3/H_s	−0.004	0.141	0.007	0.137
Pitch	$\eta_5 L/(2\pi H_s)$	0.002	0.097	0.003	0.096
Shear force	$V_3/(\rho g H_s BL)$	0.0018	0.0097	0.0014	0.0080
Bending moment	$V_5/(\rho g H_s BL^2)$	−0.0007	0.0030	−0.0006	0.0030

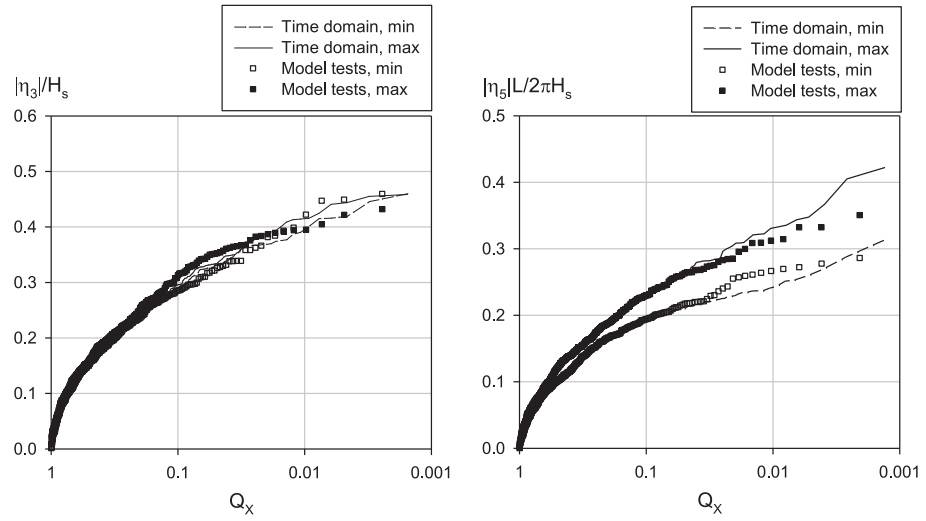

Fig. 17. Exceedance probabilities (Q_x) of heave and pitch in sea state H_s=9.0 m and T_z=10.5 s in head seas at Fn=0.0.

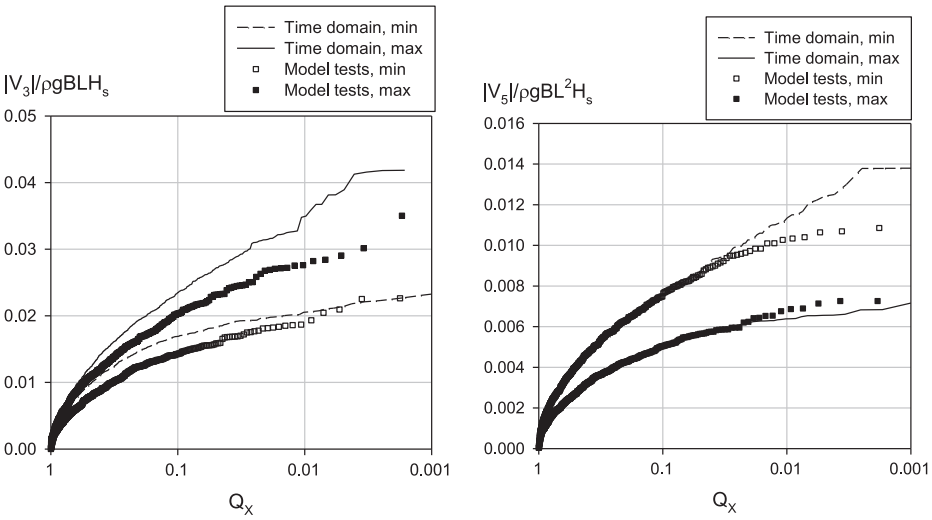

Fig. 18. Exceedance probabilities (Q_x) of shear force and bending moment in sea state H_s=9.0 m and T_z=10.5 s in head seas at Fn=0.0.

irregular sea states in the time domain calculation was about 3 h and in the model tests about 1.6 h. The mean and standard deviation of the responses are shown in Table 2. The standard deviations of heave and pitch in the calculation and model tests are close to each other. The standard deviation of the bending moment is the same. However, the shear force is about 20% bigger in the calculation than in the model tests. The exceedance probabilities of heave and pitch are presented in Fig. 17 and the shear force and bending moment are shown in Fig. 18. In the sagging condition, the bending moment is negative (minimum) and the shear force is positive (maximum). The peak distributions of heave and pitch follow the model test results well. The sagging bending moment deviates at small exceedance probability levels from the model test results. The peak distribution of the shear force is at a higher level in the sagging condition in the calculation than in the model tests and there are also differences in the hogging condition. Hence, heave and pitch are well predicted by the time domain calculation method in irregular waves. The bending moment is also well predicted but there are differences in the shear force predictions. Possible reasons for this may include inaccuracies in the load predictions on the bow and perhaps the different longitudinal mass distribution in the model tests and calculations. The loads on the bow can have a greater effect on the shear forces at the foreship than for the bending moment at midship.

4. Conclusions

A time domain calculation method for nonlinear hydrodynamic loads of floating bodies in waves is presented. The perturbation velocity potential is solved using source distributions on the body surface. The source distributions are represented by means of the transient Green function. The time derivative of the velocity potential in Bernoulli's equation is solved using an acceleration potential method. In the acceleration potential method, a potential function is solved with a similar source formulation to that of the perturbation velocity potential. The acceleration potential method gives a reliable and stable solution for the responses.

For the Wigley hull form, the comparison between the existing experimental results and the time domain method shows good agreement of added mass damping coefficients, and the heave and pitch motions. Furthermore, the time domain method was applied to predict responses for the RoPax ship and the calculated predictions were compared with the model test results. In calm water, the model test results show that the steady bending moment and shear force increase if the forward speed increases. The calculated results are in good agreement with the model test results but the uncertainty of the calculated predictions increases if the forward speed increases. For the model test ship, the steady hull girder loads are in the order of 10% of the still water loads at forward speed $Fn=0.25$. The model test results show that differences between the sagging and hogging shear force and the bending moment in regular and irregular head waves are significant for the RoPax ship. The time domain method can predict the nonlinearities in the sagging and hogging shear forces and bending moments. At zero speed, the time domain method gives good predictions for the bending moment, but the differences for the shear force were larger comparing to the model test results.

Further studies are needed to investigate the effect of the bow and stern impact loads on the hull girder loads and dynamic responses. The calculation method should also be verified and validated in oblique waves.

Acknowledgements

This research project was funded by the Finnish Funding Agency for Technology and Innovation (Tekes), the Finnish Navy, STX Finland, SWECO and Technip Finland Offshore. This financial support is gratefully acknowledged.

References

Bandyk, P.J., Beck, R.F., 2011. The acceleration potential in fluid-body interaction problems. J. Eng. Math. 70, 147–163.
Batchelor, G.K., 1967. An Introduction to Fluid Dynamics. Cambridge University Press, ISBN: 978-0-521-66396-0.
Beck, R., Reed, A., 2000. Modern seakeeping computations for ships. In: Proceedings of the 23rd Symposium on Naval Hydrodynamics, Office of Naval Research ONR.
Dai, Y.Z., Wu, G.X., 2008. Time domain computation of large amplitude body motion with the mixed source formulation. In: Eighth International Conference on Hydrodynamics, Nantes.
Datta, R., Rodrigues, J.M., Guedes Soares, C., 2011. Study of the motions of fishing vessels by a time domain panel method. Ocean Eng 38, 782–792.
Drummen, I., Wu, M.K., Moan, T., 2009. Experimental and numerical study of containership responses in severe head seas. Mar. Struct. 22, 172–193.
Duan, W., Dai, Y., 1999. Time-domain calculation of hydrodynamic forces on ships with large flare (Part 1: Two-dimensional case and Part 2: Three-dimensional case). Int. Shipbuild. Prog. 46 (446), 209–233.
Ferrant, P., 1991. A coupled time and frequency approach for nonlinear radiation. In: 18th Symposium on Naval Hydrodynamics, pp. 67–83.
Fonesca, N., Guedes Soares, C., 1998. Time-domain analysis of large-amplitude vertical ship motions and wave loads. J. Ship Res. 42 (2), 139–153.
Greco, M., 2001. A Two-dimensional Study of Green-Water Loading. Ph.D. Thesis. Department of Marine Hydrodynamics Faculty of Marine Technology, Norwegian University of Science and Technology, Trondheim, Norway.
Huang, Y., Sclavounos, P., 1998. Nonlinear ship motions. J. Ship Res. 42 (2), 120–130.
ITTC, 2002. The Specialist Committee on Waves. Final Report and Recommendations to the 23rd ITTC. 23rd International Towing Tank Conference, Proceedings of the 23rd ITTC—Volume II.
Journee, J.M.J., 1992. Experiments and Calculations on Four Wigley Hullforms. TU Delft, MEMT 21.
Jensen, J.J., Pedersen, P.T., Shi, B., Wang, S., Petricic, M., Mansour, A., 2008. Wave induced extreme hull girder loads on containerships. Trans. SNAME 116, 128–152.
Kang, C.-G., Gong, L.-Y., 1990. A numerical solution method for three-dimensional nonlinear free surface problems. In: Proceedings of the 18th Symposium on Naval Hydrodynamics, pp. 427–438.
Kataoka, S., Sueyoshi, A., Arihama, K., Iwashita, H., Takaki, M., 2002. A study on body non-linear effects on ship motions. Trans. West Jpn. Soc. Naval Archit. 104, 111–120. (in Japanese).
Kataoka, S., Iwashita, H., 2004. Estimations of hydrodynamic forces acting on ships advancing in the calm water and waves by a time-domain hybrid method. J. Soc. Naval Archit. Jpn. 196, 123–138. (in Japanese).
Koo, W, Kim, M.-H., 2004. Freely floating-body simulation by a 2D fully nonlinear numerical wave tank. Ocean Eng 31, 2011–2056.
Kukkanen, T., 2012. Numerical and Experimental Studies of Nonlinear Wave Loads of Ships. Doctoral Thesis. VTT Science 15. Available at: ⟨http://www.vtt.fi/inf/pdf/science/2012/S15.pdf⟩.
Liapis, S., Beck, R., 1985. Seakeeping computations using time-domain analysis. In: Proceedings of the Fourth International Conference on Numerical Ship Hydrodynamics, pp. 34–54.
Lin, W.-M., Yue, D., 1991. Numerical solution for large-amplitude ship motions in the time domain. In: 18th Symposium on Naval Hydrodynamics, pp. 41-66.
Milne-Thomson, L.M., 1968. Theoretical HydrodynamicsDover Publications (1996), ISBN: 0-486-68970-0.
Newman, J.N., 1992. Approximation of free-surface Green functions. Wave Asymptotics, 107–135. Cambridge University Press.
Pawlowski, J., 1992. A nonlinear theory of ship motions in waves. In: Proceedings of the 19th Symposium on Naval Hydrodynamics, pp. 33–57.
Sen, D., 2002. Time-domain computation of large amplitude 3D ship motions with forward speed. Ocean Eng 29, 973–1002.
Song, M.-J., Kim, K.-H., Kim, Y., 2011. Numerical analysis and validation of weakly nonlinear ship motions and structural loads on a modern containership. Ocean Eng 38, 77–87.
Tanizawa, K., 1995. A nonlinear simulation method of 3-D body motions in waves (1st report). Formulation with the Acceleration Potential. J. Soc. Naval Archit. Jpn. 178, 179–191.
Vinje, T., Brevig, P., 1981. Nonlinear ship motions. In: The Proceedings of the Third International Conference on Numerical Ship Hydrodynamics, pp. 257–268.
Weems, K.M., Lin, W.M., Zhang, S., Treakle, T., 2000. Time domain prediction for motions and loads of ships and marine structures in large seas using a mixed-singularity formulation. In: Proceedings of the Fourth Osaka Colloquium on Seakeeping Performance of Ships (OC2000), Osaka, Japan, pp. 272–280.
Wehausen, J.V., Laitone, E.V., 1960. Surface waves. Encyclopedia of physics. Fluid Dynamics III, vol. IX. Springer-Verlag, pp. 446–778.
Wu, G.X., Eatock Taylor, R., 1996. Transient motion of a floating body in steep water waves. In: The 11th International Workshop on Water Waves and Floating Bodies, Germany.
Wu, G.X., 1998. Hydrodynamic force on a rigid body during impact with liquid. J. Fluids Struct. 12, 549–559.
Wu, M.K., Moan, T., 1996. Linear and nonlinear hydroelastic analysis of highspeed vessels. J. Ship Res. 40 (2), 149–163.
Wu, M.K., Moan, T., 2005. Efficient calculation of wave-induced ship responses considering structural dynamic effects. Appl. Ocean Res. 27, 81–96.
Zhang, X., Bandyk, P., Beck, R.F., 2010. Time-domain simulations of radiation and diffraction forces. J. Ship Res. 54 (2), 79–94.
Zhu, S., Wu, M.K., Moan, T., 2011. Experimental and numerical study of wave-induced load effects of open ships in oblique seas. J. Ship Res. 55 (2), 100–123.